Stanford Exploration Project, Report 102, October 25, 1999, pages 1–60

Enhancing common-image gathers with prestack Stolt residual migration

Paul Sava[1]

keywords: *residual migration, Stolt, velocity analysis, CIG*

ABSTRACT

Wave-equation migration velocity analysis is a two-step process: first, we estimate the perturbation between a starting image and a better-focused image, and then invert for the perturbation in slowness that explains the perturbation in image obtained in the first step. The key to success is to obtain a sharp image, with flat common-image gathers at every location. In this paper, I show how prestack Stolt residual migration and common-image gathers come together, and lead to a successful image enhancement procedure with which we can transform a given image into a better-focused one.

INTRODUCTION

Wave-equation migration velocity analysis (Biondi and Sava, 1999) has recently emerged as a promising new technology with the potential to overcome the difficulties encountered in complex structures by traveltime-based velocity analysis methods.

Briefly, in wave-equation migration velocity analysis (WEMVA), we iteratively update the slowness model with perturbations in slowness (ΔS) obtained by inversion from perturbations in image (ΔR), which, by definition, is the difference between the current image and a better-focused image (Figure 1). The key ingredient of WEMVA is the better-focused image with which we compare the original image. Here, residual migration plays a very important role, because it has remarkable properties of image enhancement.

Several residual migration methods are capable of improving the migrated images. A good choice is Stolt prestack residual migration, which is not only fast and robust, but can also be formulated as a velocity-independent procedure (Sava, 1999).

Another important element of WEMVA is the ability to convert images to angle-domain common-image gathers (Prucha et al., 1999) to assess the quality of the velocity used in imaging. When the velocity is incorrect, different events in CIGs are not flat, but rather point up or down, and therefore are a very clear guide to where and how the velocity map needs improvement.

[1]**email:** paul@sep.stanford.edu

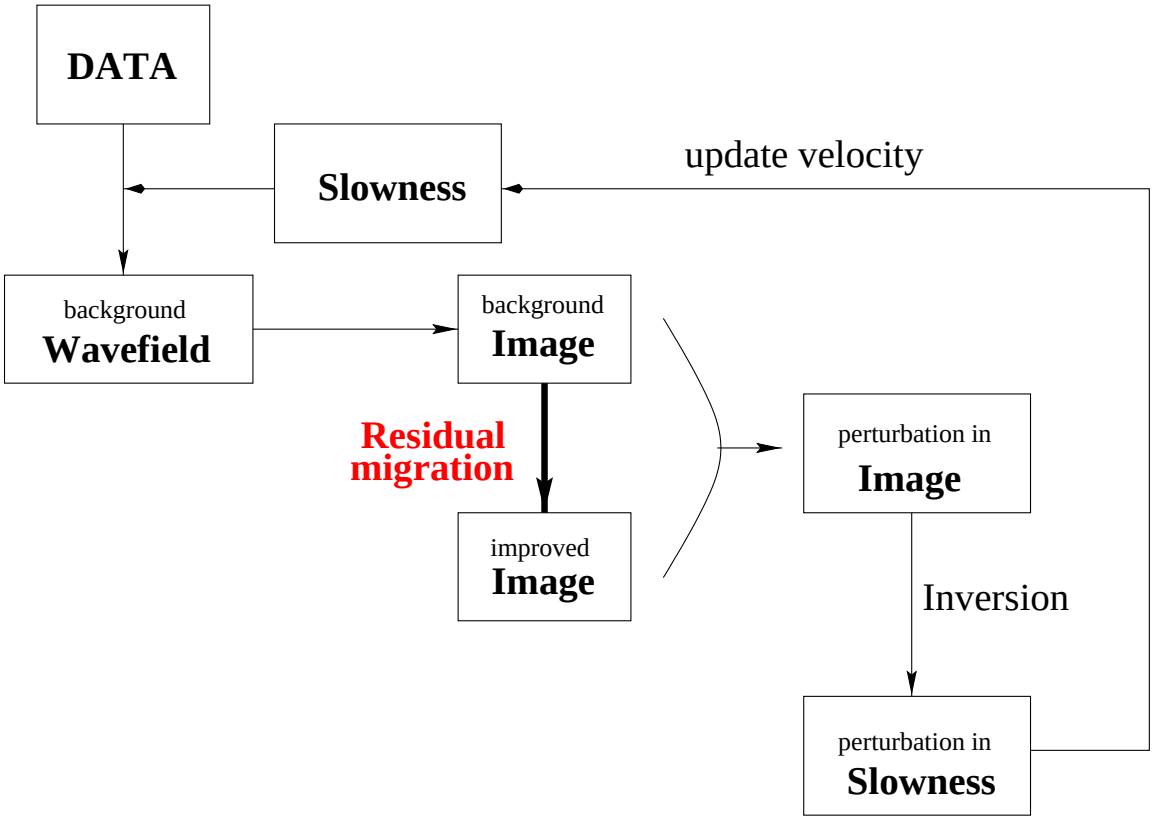

Figure 1: WEMVA flow chart. We start with the recorded data and an initial guess about the slowness model (background slowness). We compute the background wavefield by recursive downward continuation from the surface and image (background image). We then apply an image enhancement procedure (residual migration) to get a better-focused image. From the two images we compute the perturbation in image, which we can invert for the perturbation in slowness. Finally, we update the background slowness and repeat the loop until convergence is achieved. paul1-flow [NR]

In this paper, I present an example of how residual migration can be used to improve the quality of images. I use a synthetic model with features relevant to real data in complex structures: dipping beds, reverse faults, and zones of severe distorsion. Throughout the project, I make extensive use of angle-domain CIGs.

IMAGE ENHANCEMENT THEORY

Residual migration has proved to be a useful tool in imaging and in velocity analysis. Recent publications show that Stolt residual migration can be applied in the prestack domain (Stolt, 1996), and, furthermore, that it can be posed as a velocity-independent process (Sava, 1999). Consequently, we can use Stolt residual migration in the prestack domain to obtain a better-focused image without making any assumption about the velocity. This is why Stolt residual migration in the prestack domain appears to be a good choice for image enhancement after wave-equation migration.

Strictly speaking, Stolt prestack residual migration is a constant velocity process. However, with this process we obtain images that correspond to velocities that have a given *ratio* to the original one. Therefore, if the original velocity is variable, the new velocities are also not constant, but only slightly faster or slower than the reference. The true relationship between the original and new velocities is still not fully understood, and remains a subject for future research.

One possible measure of the degree to which the prestack image is focused is the flatness of the angle-domain common-image gathers (CIG) (Biondi, 1999; Prucha et al., 1999). An accurate velocity model is a sufficient condition for the CIGs to be flat. Once the CIGs are flat, summation of the flat events along the aperture-angle axis yields high-energy stacks, while summation along the nonflat events yields lower energy stacks.

The angle-domain common-image gathers are representations of the depth images in a coordinate system defined by depth, midpoint, and aperture-angle. The aperture-angles can be computed in the wavenumber domain as a function of the offset and depth wavenumbers (k_h, k_z) as [2]

$$a_h = \arctan\left(\frac{k_h}{k_z}\right). \tag{1}$$

There are two major reasons for the representation of the angle-domain CIGs with the aperture-angle as the "offset" axis:

- The representation in aperture-angle contains valuable information for velocity analysis through the strong moveout of the events migrated with incorrect velocity (Prucha et al., 1999), as shown in Figure 7. This property is also true when we represent the CIGs as a function of the offset ray-parameter (p_h).

[2]Computing the aperture-angle with the equation (1) assumes that the reflection happens in the inline direction and that there is no azimuthal component to it. This assumption is correct in the 2-D case I analyze in this paper, but it is still an open question when dealing with 3-D data.

- Angle-domain CIGs where the angle axis is described through the offset ray-parameter (p_h) require knowledge about the velocity field. This is fine if we compute the CIGs after wave-equation depth migration. However, it is much more difficult to assess the correct velocity of the images that have been obtained by residual migration. It is, at least for this application, better to replace p_h with a_h, as defined in the preceding equation.

We can use the information contained in the CIGs to generate better focused images from a suite of images obtained through residual migration for different ratios between the original and modified velocities (Sava, 1999). Since the velocity model is not constant, different ratios will flatten the events more or less in different regions of the image. It follows that the energy of the stack will also vary with the ratio at every location in the image. Therefore, we can pick a map of ratios that represents the highest energy stack, and implicitly the flattest CIGs. At the same time, we can also extract the image that corresponds to the highest energy. In the rest of the paper, I call this image the best focused image.

The full image-enhancement procedure is outlined in the flow-chart shown in Figure 2.

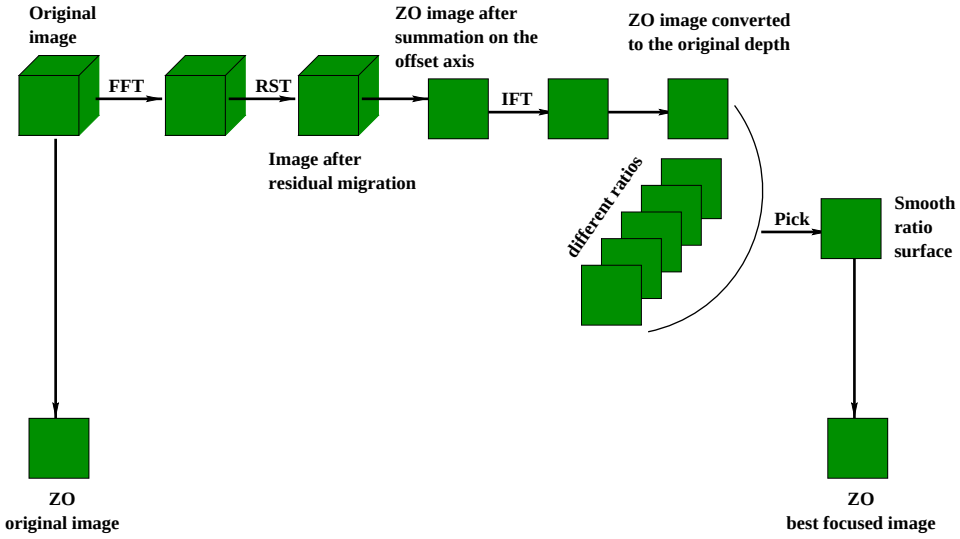

Figure 2: Image enhancement flowchart. We start with the prestack original image, Fourier transform it on all axes, apply residual migration with a given ratio, sum over the offset axis to obtain the zero-offset (ZO) image, and convert it to the original depth. We then repeat the same procedure to obtain ZO images for a suite of ratios and pick the maximum energy. Finally, we compare the ZO section before residual migration to the best focused ZO section after residual migration and optimal picking. paul1-pick [NR]

RESULTS

This section offers an example of image enhancement using prestack Stolt residual migration. Figures 3 and 4 show the reflectivity and the slowness model I consider in this example.

The model poses imaging difficulties because of the fast layer that is moved up along the reversed fault. Since the velocity in the layer is much faster than that of the surrounding material, the image under the upper section is expected to be heavily distorted when imaged with an approximate velocity. An easy way to highlight the distorsion zone is through wavefront tracing (Sava and Fomel, 1997), which has been shown to approximate wave propagation very well, even in regions of high velocity contrast (Figure 5).

Such a model is especially relevant for regions with large velocity contrasts and steeply dipping boundaries, for example in the North Sea (Vaillant and Sava, 1999) or the Gulf of Mexico, around salt domes. Dipping events tend to move laterally at every offset when imaged with different velocities; therefore residual imaging processes that do not take into account this lateral movement, like residual move-out or warping (Rickett and Lumley, 1998), cannot fully correct the image, but can only increase the flatness of the CIGs. Although flat CIGs are a necessary condition for a correct image, they are not a sufficient one.

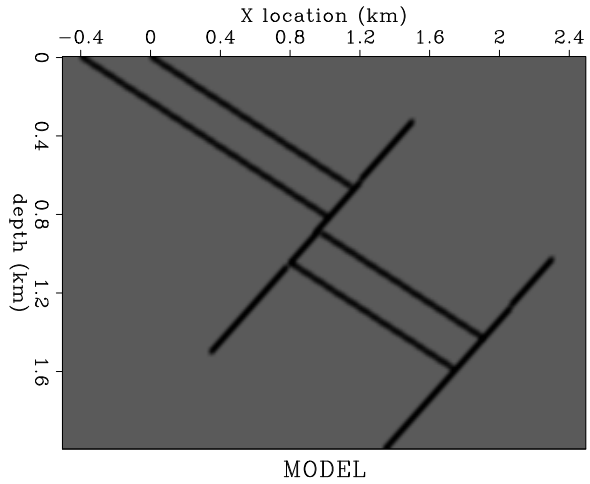

Figure 3: The reflectivity model. paul1-model [ER]

First, I generate the data corresponding to an acquisition with a cable 3.2 km long (Figure 6). I then perform wave-equation modeling using an extended split-step algorithm (Stoffa et al., 1990; Biondi and Palacharla, 1996) to generate data, starting from the reflectivity map and the true slowness.

The next step is to create a starting image for the residual migration process by migrating the data with an approximate slowness model, obtained by removing the fast layers and smoothing the model laterally and vertically. The assumption I make is that even if we do not know much about the fast layer, we have a pretty good idea of the velocities on both sides of the fault.

Finally, in the residual migration step, I generate a suite of 41 images corresponding to velocity ratios (ρ) ranging from 0.9 to 1.1 (Figure 8). The values of ρ smaller than 1.0 correspond to new velocities that are higher than the original, while the values above 1.0 correspond to new velocities lower than the original (Sava, 1999).

By studying the different ρ images, we can identify two types of events:

- The first are the mildly dipping events, for example the layers, which do not show

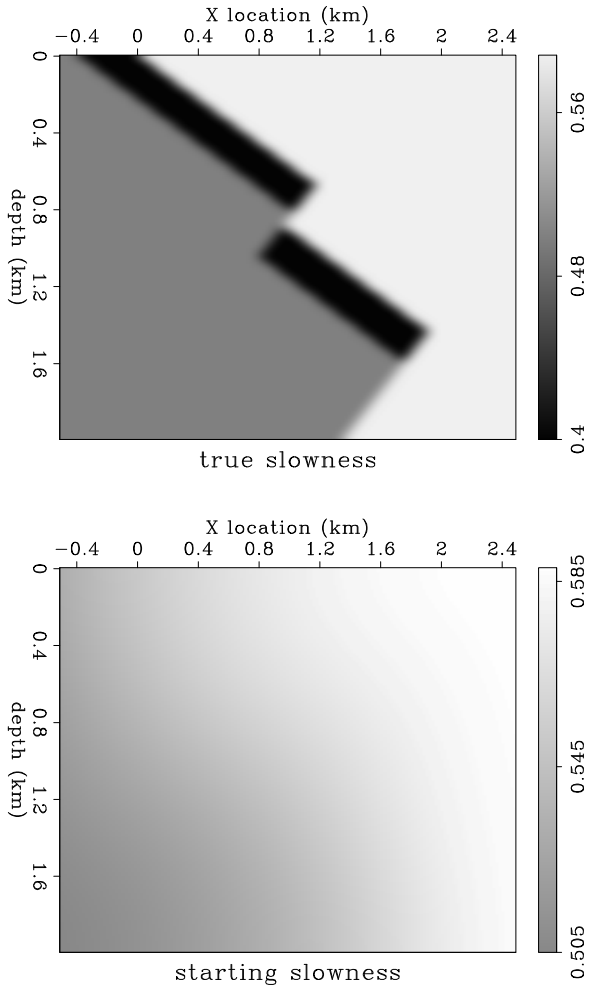

Figure 4: The slowness maps. The upper panel is the true slowness used to generate the data (Figure 6). The lower panel is the smooth slowness I used to create the starting image (Figure 7). The smooth model is obtained by heavily smoothing the true slowness model, with the fast layer removed. paul1-slow [ER]

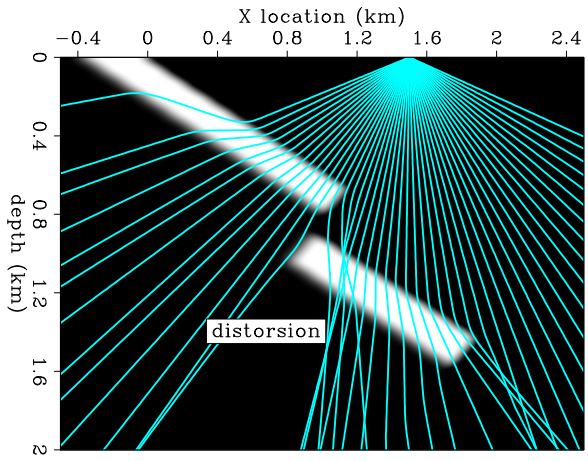

Figure 5: A zone of distorsion is created by the fault and the upper segment of the fast layer. paul1-rays [ER]

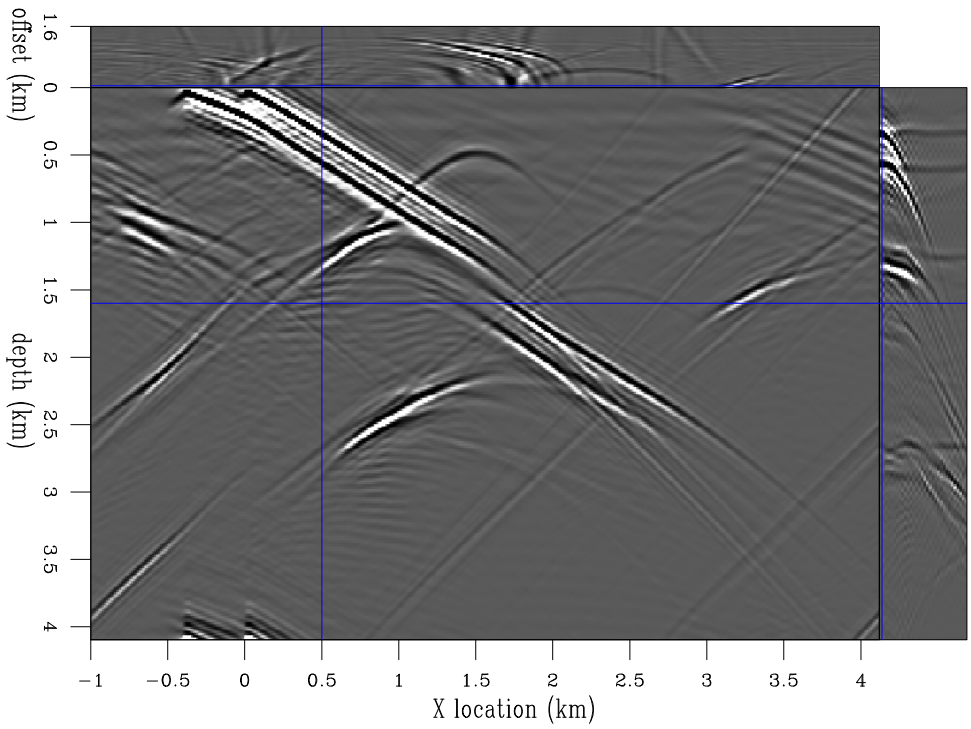

Figure 6: The data generated by wave-equation modeling from the reflectivity model (Figure 3) and the true slowness (upper panel in Figure 4). paul1-data [ER]

large lateral movement, but only changes in the moveout of the CIGs. We can obtain better images for these events simply by flattening the CIGs (residual moveout does a reasonably good job).

- Dipping events, such as the fault, which shows significant lateral movement (Figure 8), focus/defocus and present large moveouts in the CIGs. For these events, residual moveout is not appropriate, because it is not enough to flatten an event that is not in its right position. We need to use the more sophisticated procedure of residual migration.

Finally, I stack all these images along their aperture-angle axis, and pick the smooth surface that goes through the points of maximum energy (Figure 10). Once I obtain the surface, I can cut through the stacked slices (Figure 9) and extract the better-focused image (Figure 11).

A simple visual analysis of the images before and after residual migration reveals the areas of improvement. First, the segment of the fault below the fast layer (labeled A in Figure 11) moves toward its correct position to the right, and in better alignment with the segment above the fault. Also, we can clearly identity the better focusing of the reflectors situated in the shadow zone (labeled B and C in Figure 11). These two events are also more closely aligned with their ideal location (Figure 3).

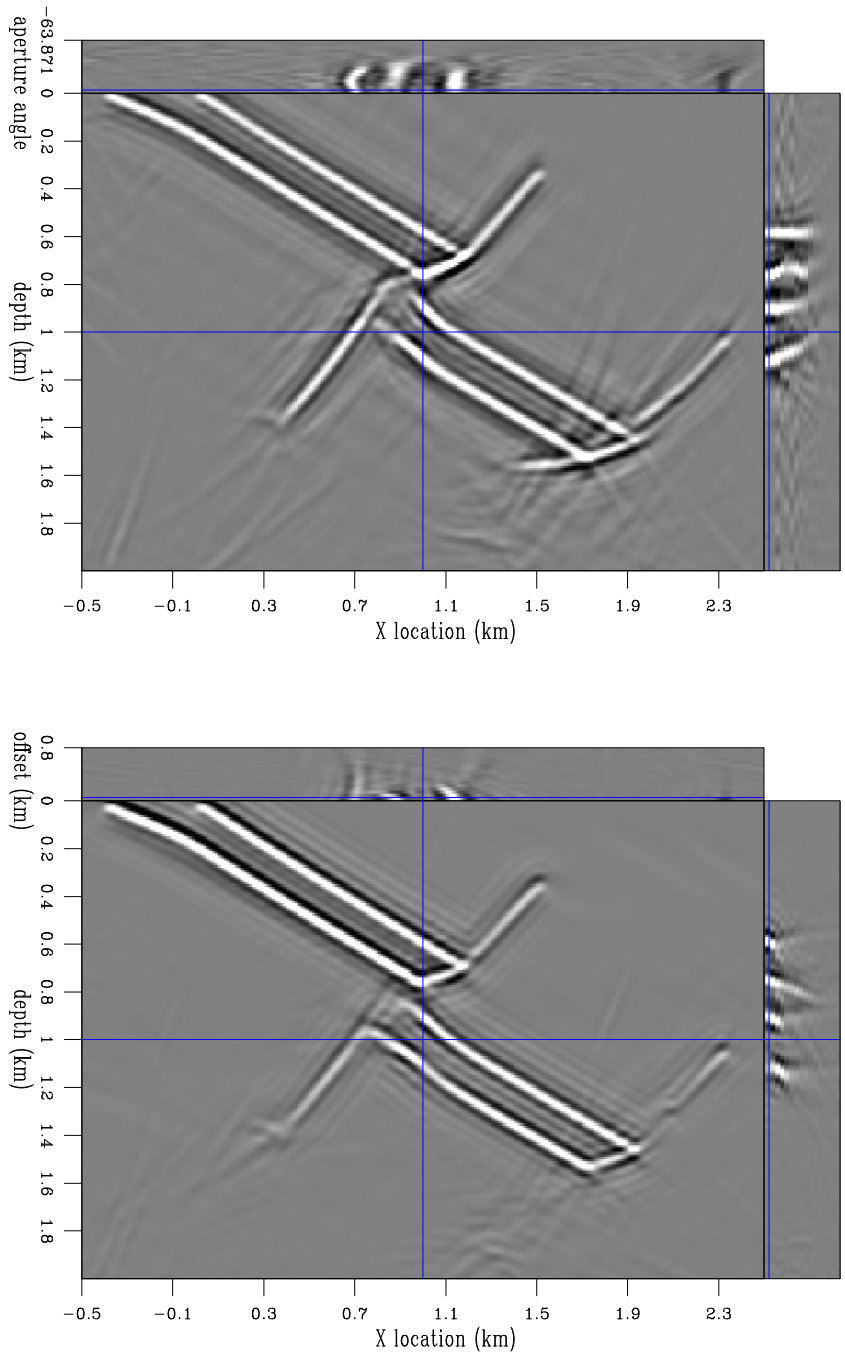

Figure 7: The image obtained by wave-equation migration with the wrong slowness model (Figure 4). The upper plot represents common-image gathers (where the third axis is the aperture-angle), while the bottom plot represents the same information as a function of offset. Properly migrated data should show flat events in the common-image gathers. Events pointing up are a sign of under-migration, while events pointing down are a sign of over-migration. The events with gathers pointing both up and down correspond to the situation when the near and far offsets are influenced by different types of perturbation in the velocity field. The images are not directly comparable, because in the CIG version more of the energy present at the near offsets is spread along the aperture-angle axis, and therefore some events become relatively stronger. paul1-imageF [ER]

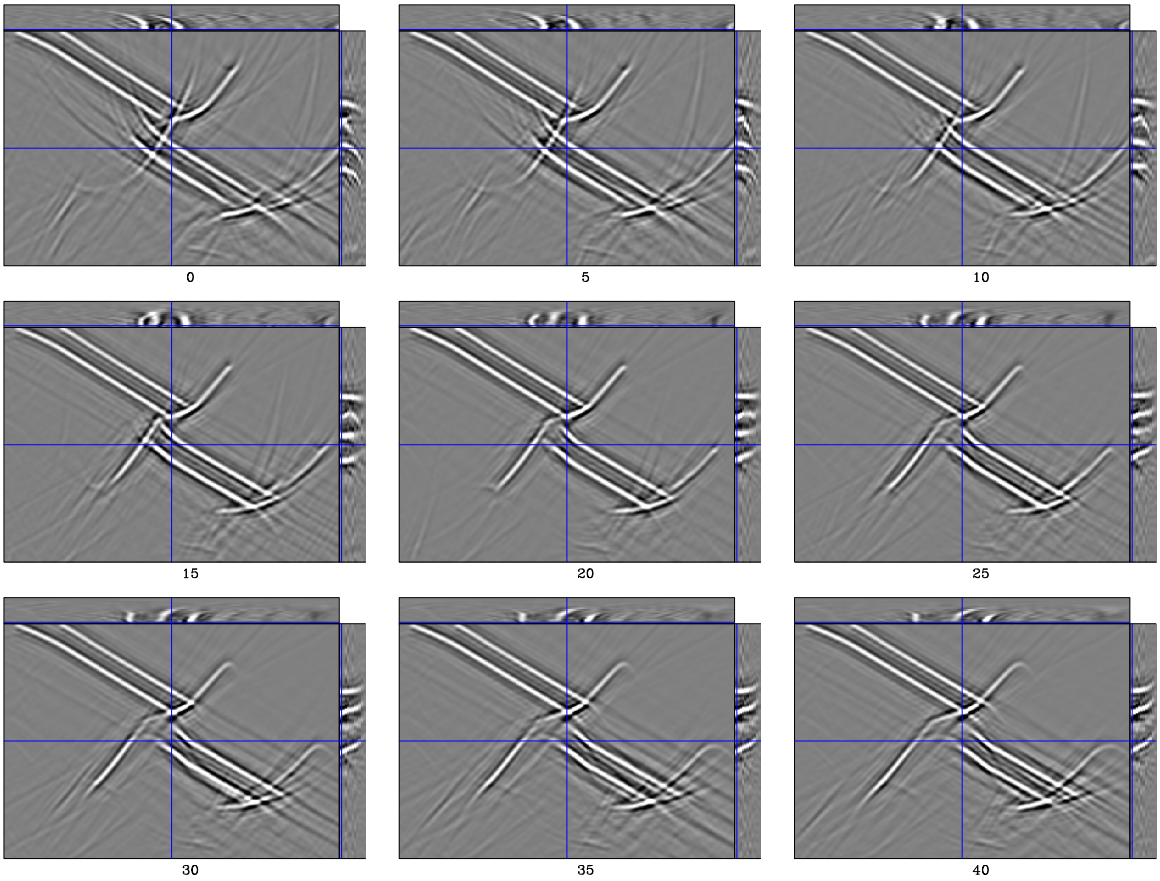

Figure 8: The images obtained after residual migration. Each panel corresponds to a different residual migration ratio (ρ), as follows: 0($\rho = 0.9$), 5($\rho = 0.925$), 10($\rho = 0.95$), 15($\rho = 0.975$), 20($\rho = 1.0$), 25($\rho = 1.025$), 30($\rho = 1.05$), 35($\rho = 1.075$), 40($\rho = 1.1$). The values of ρ smaller than 1.0 correspond to new velocities that are higher than the original, while the values above 1.0 correspond to new velocities lower than the original. The panel labeled 20 is the original image (Figure 7) with no residual migration ($\rho = 1.0$). paul1-resmig [ER]

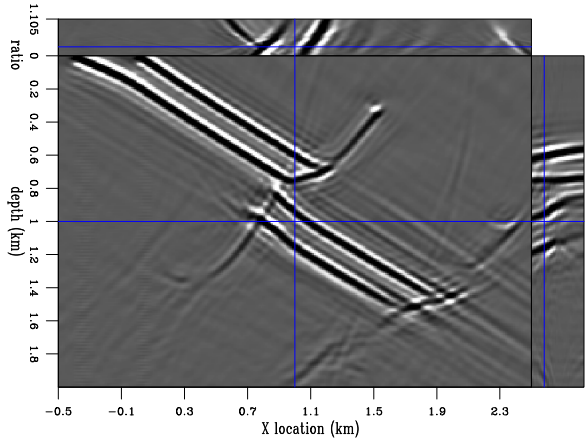

Figure 9: The cube of stacked sections. Each plane represents an image at a given ratio. We can use this cube to extract both the surface of maximum energy, and the optimally focused image. Each stack has been converted to the original depth to reduce the vertical movement from one ratio to the other. paul1-stack [ER]

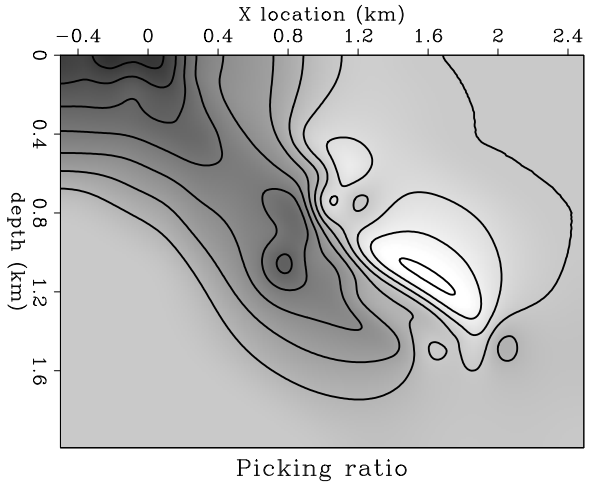

Figure 10: The surface of the picking ratio. This surface represents the values of the ratio (ρ) for which the events are flattest at every point in the common-image gathers. The flatness is measured by the energy of the stack along the angle of incidence axis – the flatter the event, the higher the energy. Dark colors represent values of ρ smaller than 1, while lighter colors represent values of ρ higher than 1. Contours are drawn at every 0.01 units on the ratio axis. paul1-surface [ER]

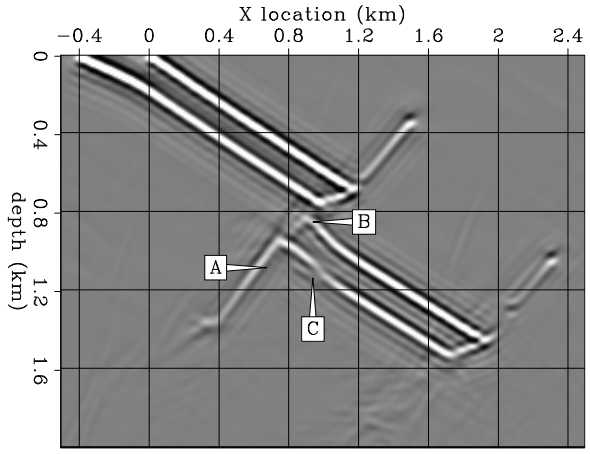

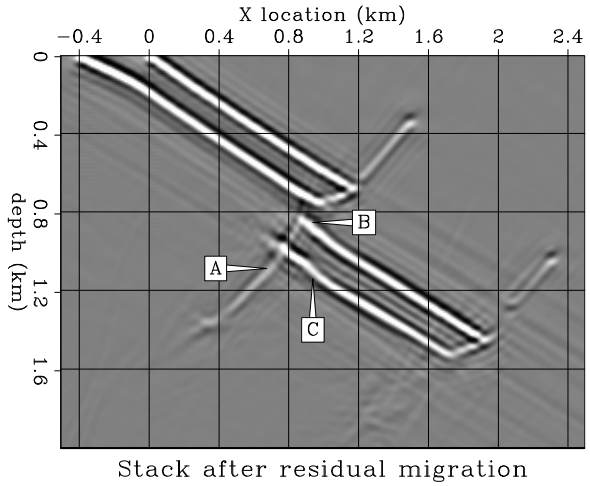

Figure 11: A comparison between the original image obtained through migration with the wrong velocity (Figure 7) and the improved image obtained after residual migration and picking using the best-focusing surface (Figure 10). The area of interest is located at the horizontal location $0.7 - 1.1$ km and depth $0.8 - 1.0$ km. The segment of the fault in the shadow of the fast layer is moved to the right toward its correct position (A). The top reflectors (B and C), also in the shadow of the fast layer, are moved almost to their correct position and are much more energetic in the best-focused image (below) than in the original image (above). paul1-improved [ER]

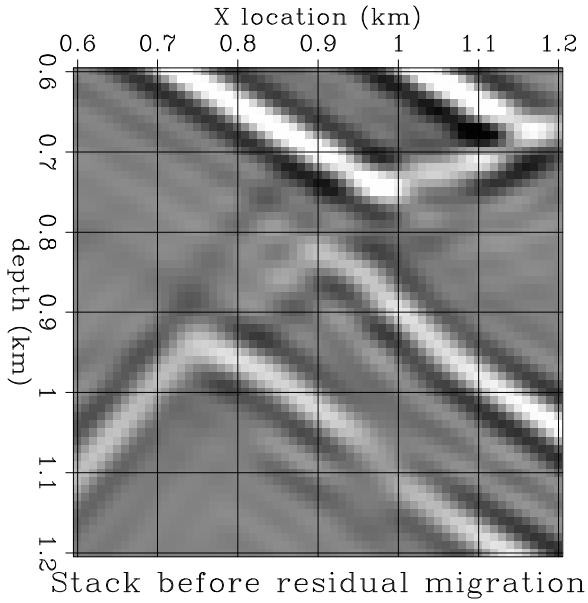

Figure 12: Same comparison as in Figure 11. Zoom over the zone of interest. paul1-detail [ER]

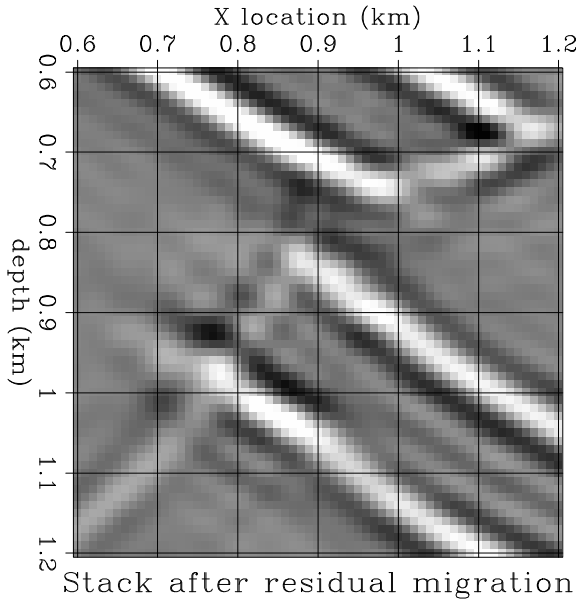

CONCLUSIONS

Velocity-independent Stolt residual migration improves the image focusing for a model with significance for seismic imaging problems in areas of large velocity contrast and limited illumination. In this study I have found that residual migration is applicable and can generate better-focused images. The entire process is cheap, with a cost comparable with that of a suite of Stolt migrations.

The potential pitfalls occur in the area of maximum energy picking. Complex situations, where different events cross along the ratio direction, pose a significant challenge for the automated picker. Better picking algorithms, or maybe interactive techniques, can resolve this problem. This is an area for future work, together with more experiments on both real and synthetic data.

Another direction for future work, with more relevance to velocity analysis, is the extension of the current method to prestack data and to 3-D common-azimuth data. Once we have obtained the picking surface, we can cut directly though the prestack images to get the one with the best focusing and the flattest CIGs.

ACKNOWLEDGMENTS

I would like to thank Biondo Biondi for numerous and stimulating discussions. I would also like to thank James Rickett for providing a most welcome challenge.

REFERENCES

Biondi, B., and Palacharla, G., 1996, 3-D prestack migration of common-azimuth data: Geophysics, **61**, no. 6, 1822–1832.

Biondi, B., and Sava, P., 1999, Wave-equation migration velocity analysis: SEP–**100**, 11–34.

Biondi, B., 1999, Subsalt imaging by common-azimuth migration: SEP–**100**, 113–124.

Prucha, M. L., Biondi, B. L., and Symes, W. W., 1999, Angle-domain common image gathers by wave-equation migration: SEP–**100**, 101–112.

Rickett, J., and Lumley, D., 1998, A cross-equalization processing flow for off-the-shelf 4-D seismic data: SEP–**97**, 265–274.

Sava, P., and Fomel, S., 1997, Huygens wavefront tracing: A robust alternative to conventional ray tracing: SEP–**95**, 101–113.

Sava, P., 1999, On Stolt prestack residual migration: SEP–**100**, 151–158.

Stoffa, P. L., Fokkema, J. T., de Luna Freire, R. M., and Kessinger, W. P., 1990, Split-step Fourier migration: Geophysics, **55**, no. 4, 410–421.

Stolt, R. H., 1996, Short note–a prestack residual time migration operator: Geophysics, **61**, no. 2, 605–607.

Vaillant, L., and Sava, P., 1999, Common-azimuth migration of a north sea dataset: SEP–**102**, 1–14.